LETTERS
PUBLISHED ONLINE: 17 JUNE 2012 | DOI: 10.1038/NNANO.2012.96
nature nanotechnology

Control of valley polarization in monolayer MoS_2 by optical helicity

Kin Fai Mak[1], Keliang He[2], Jie Shan[2] and Tony F. Heinz[1]*

Electronic and spintronic devices rely on the fact that free charge carriers in solids carry electric charge and spin. There are, however, other properties of charge carriers that might be exploited in new families of devices. In particular, if there are two or more minima in the conduction band (or maxima in the valence band) in momentum space, and if it is possible to confine charge carriers in one of these valleys, then it should be possible to make a valleytronic device[1–4]. Valley polarization, as the selective population of one valley is designated, has been demonstrated using strain[5,6] and magnetic fields[7–10], but neither of these approaches allows dynamic control. Here, we demonstrate that optical pumping with circularly polarized light can achieve complete dynamic valley polarization in monolayer MoS_2 (refs 11,12), a two-dimensional non-centrosymmetric crystal with direct energy gaps at two valleys[13–16]. Moreover, this polarization is retained for longer than 1 ns. Our results, and similar results by Zeng *et al.*[17], demonstrate the viability of optical valley control and suggest the possibility of valley-based electronic and optoelectronic applications in MoS_2 monolayers.

Optical photons do not carry significant momentum, so they cannot selectively populate different valleys based on this attribute. In certain materials, however, carriers in different valleys are associated with well-defined, but different angular momenta. This suggests the possibility of addressing different valleys by controlling the photon angular momentum, that is, by the helicity (circular polarization state) of light. Indeed, just such valley-specific circular dichroism of interband transitions has been predicted in non-centrosymmetric materials[3,4,11,12]. Graphene, with its two prominent K and K′ valleys, has been considered theoretically in this context[3,4]. For this approach to be applicable, however, the inherent inversion symmetry of the single- and bilayer graphene must be broken[3,4], and the effect has not yet been realized experimentally. Monolayer MoS_2, on the other hand, is a direct-bandgap semiconductor[13–16] that has a structure similar to graphene, but with explicitly broken inversion symmetry. It has recently been proposed as a suitable material for valleytronics[11,12].

Monolayer MoS_2 consists of a single layer of molybdenum atoms sandwiched between two layers of sulphur atoms in a trigonal prismatic structure[18] (Fig. 1a). Inversion symmetry is broken because the two sublattices are occupied, respectively, by one molybdenum and two sulphur atoms. At the K and K′ valleys in momentum space, the highest-energy valence bands and the lowest-energy conduction bands are mainly of molybdenum *d*-orbital character[18]. Because of the broken inversion symmetry, spin–orbit interactions split the valence bands by ~160 meV (refs 11,19,20) (Fig. 1b). The spin projection along the *c*-axis of the crystal, S_z, is well defined and the two bands are of spin down ($E_\downarrow$) and spin up ($E_\uparrow$) in character. This broken spin degeneracy, in combination with time-reversal symmetry ($E_\downarrow(\mathbf{k}) = E_\uparrow(-\mathbf{k})$, where $\mathbf{k}$ is crystal momentum), implies that the valley and spin of the valence bands are inherently coupled in monolayer MoS_2 (refs 11,19,20). Consequently, interband transitions at the two valleys are allowed for optical excitation of opposite helicity incident along the *c*-axis, that is, left circularly polarized (σ_-) and right circularly polarized (σ_+) at the K and K′ valleys, respectively[11,12] (Fig. 1b). Recent studies have shown that the band-edge transitions in monolayer MoS_2 are modified by electron–hole (e–h) interactions, giving rise to A and B excitons[13,14]. The selection rules, however, carry over to the excitons (Fig. 1c), because the selection rules for valley pumping are nearly exact over a large region around the two valleys[12] as a result of the heavy *d*-band mass and the large bandgap.

We examined the electronic transitions for monolayer MoS_2 from its absorption spectrum, obtained by measuring the differential reflectance of MoS_2 samples on a substrate and the bare substrate (hexagonal boron nitride, h-BN) (Fig. 2a). The principal absorption features correspond to the A and B excitons[13,14]. The emitting states are identified in the photoluminescence spectrum (Fig. 2b for total, unpolarized emission under 2.33 eV excitation). The strongest feature around 1.9 eV arises from the A exciton complexes, including the neutral and redshifted (by ~40 meV) charged excitons (K. F. Mak *et al.*, in preparation). (The charged excitons are formed when photogenerated excitons bind to free electrons[21]. The required electrons are already present in our samples, which, as observed in transport experiments[22], are unintentionally n-doped.) Weak emission from the B exciton (2.1 eV) is also observed from hot luminescence. The feature near 1.8 eV arises from emission of defect-trapped excitons.

Figure 3a presents the polarization-resolved photoluminescence spectrum (σ_- and σ_+ components) of monolayer MoS_2, excited by σ_- radiation on resonance with the A exciton at 1.96 eV (633 nm). The spectrum consists of A exciton emission and weak emission from defect-trapped excitons. The A exciton emission is purely σ_- polarized (to experimental accuracy), and the defect emission is largely unpolarized. We quantify the degree of photoluminescence polarization by the helicity parameter

$$\rho = \frac{I(\sigma_-) - I(\sigma_+)}{I(\sigma_-) + I(\sigma_+)}$$

determined from the polarization-resolved photoluminescence intensities $I(\sigma_{-/+})$. ρ is found to be 1.00 ± 0.05 for photon energies in the range 1.90–1.95 eV and drops rapidly to ~0.05 below 1.8 eV (Fig. 3b). For comparison, we performed identical measurements on Bernal-stacked bilayer MoS_2 (Fig. 1d). A dramatically different result was observed (Fig. 3d,e), with the helicity of the A exciton emission reduced to $\rho = 0.25 \pm 0.05$. Whenever σ_+ excitation was used (not shown), the same results were obtained, but the photoluminescence helicity was consistently opposite in sign. As we discuss

[1]Departments of Physics and Electrical Engineering, Columbia University, 538 West 120th Street, New York, New York 10027, USA, [2]Department of Physics, Case Western Reserve University, 10900 Euclid Avenue, Cleveland, Ohio 44106, USA. *e-mail: tony.heinz@columbia.edu

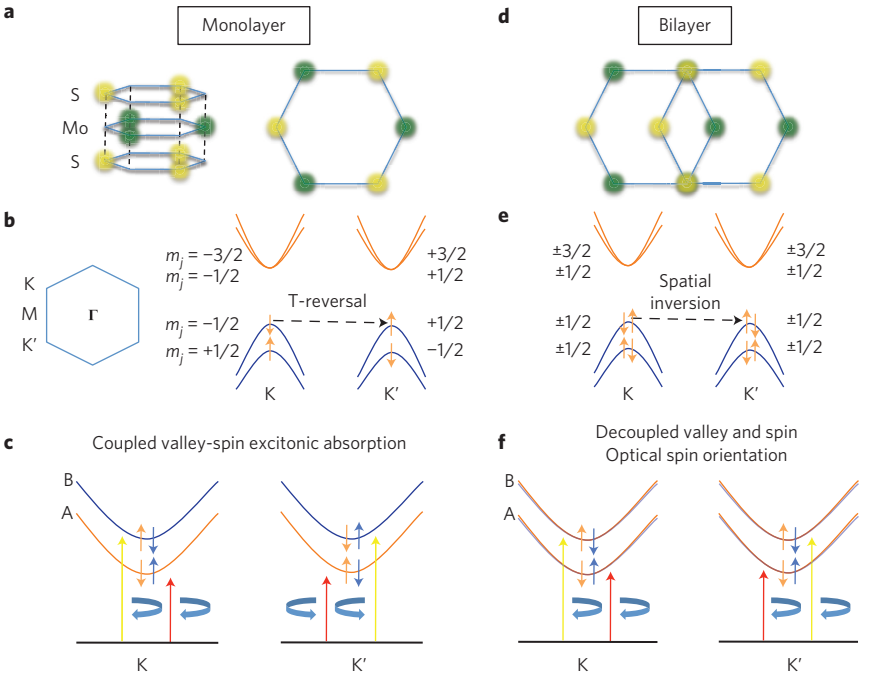

Figure 1 | Atomic structure and electronic structure at the K and K′ valleys of monolayer (a–c) and bilayer (d–f) MoS_2. a, The honeycomb lattice structure of monolayer MoS_2 with two sublattice sites occupied by one molybdenum and two sulphur atoms. Spatial inversion symmetry is explicitly broken. **b**, The lowest-energy conduction bands and the highest-energy valence bands labelled by the *z*-component of their total angular momentum. The spin degeneracy at the valence-band edges is lifted by the spin–orbit interactions. The valley and spin degrees of freedom are coupled. **c**, Optical selection rules for the A and B exciton states at two valleys for circularly polarized light. **d**, Bilayer MoS_2 with Bernal stacking. **e**, Spin degeneracy of the valence bands is restored by spatial inversion and time-reversal symmetries. Valley and spin are decoupled. **f**, Optical absorption in bilayer MoS_2. Under circularly polarized excitation (shown for σ_-) both valleys are equally populated and only a net spin orientation is produced.

below, in the absence of valley-specific excitation, the observation of full photoluminescence helicity is unexpected. The need for valley-selective excitation is further confirmed by the weakness of the photoluminescence helicity for the bilayer sample where inversion symmetry precludes such selectivity.

Photoluminescence helicity ρ reflects generally the relationship between the excited-state lifetime and the angular momentum relaxation time[23]. In our case, this corresponds to the relationship between the exciton lifetime and the hole spin lifetime[23] (Supplementary Sections S1,S3). For a quantitative treatment, we note that the helicity ρ_A of the A exciton emission in monolayer MoS_2 under on-resonance σ_- excitation is determined by the steady-state hole valley-spin population,

$$\rho_A = \frac{n_K^A - n_{K'}^A}{n_K^A + n_{K'}^A}$$

where n_K^A and $n_{K'}^A$ are, respectively, the populations of excitons in the K (hole spin up) and K′ (hole spin down) valleys. By balancing the pumping, recombination and relaxation rates of the exciton complexes, including both the neutral and charged excitons (Supplementary Section S1), we obtain, for the helicity of the neutral A and charged A^- exciton emission,

$$\rho_A = \frac{1}{1 + 2\tau_A/\tau_{AS}}, \qquad \rho_{A^-} = \rho_A \frac{1}{1 + 2\tau_{A^-}/\tau_{A^-S}} \qquad (1)$$

where $\tau_A^{-1}\left(\tau_{A^-}^{-1}\right)$ denotes the total decay rate of the neutral (charged) exciton and $\tau_{AS}^{-1}\left(\tau_{A^-S}^{-1}\right)$ is the intervalley relaxation rate of the neutral (charged) exciton. The charged exciton photoluminescence emission time is estimated to be ~5 ps according to time-resolved

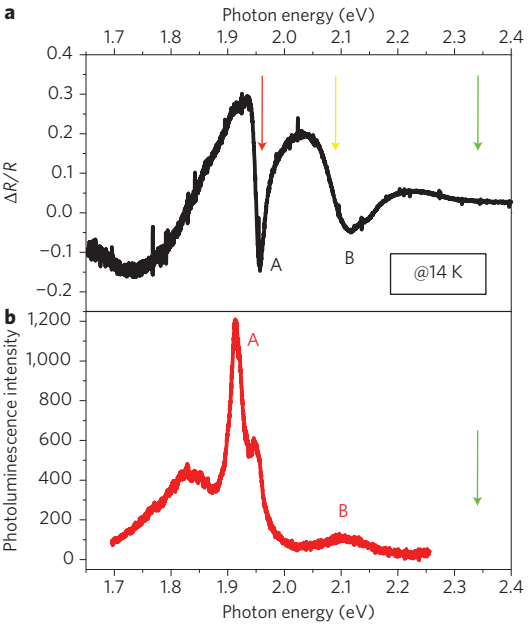

Figure 2 | Optical absorption and photoluminescence spectra of monolayer MoS_2. a, Differential reflectance spectrum showing the narrow A exciton and the broader B exciton features. Red, yellow and green arrows represent the three different photon energies used to excite the samples in the photoluminescence measurements. **b**, Photoluminescence spectrum (not polarization resolved) for 2.33 eV (532 nm) excitation. The spectrum consists of B exciton hot luminescence and A exciton luminescence (including the neutral exciton emission and the charged exciton emission, redshifted by 40 meV). The lower energy feature is attributed to trapped excitons.

photoluminescence measurements on samples on SiO_2/silicon substrates at the relevant temperatures[24]. Our samples on the h-BN substrate have over 10 times higher photoluminescence quantum yield (Supplementary Section S2), implying an exciton lifetime of >50 ps. Thus, the observation of $\rho = 1.00 \pm 0.05$ yields a hole valley-spin lifetime of >1 ns in monolayer MoS_2. On the other hand, because bilayer MoS_2 is an indirect-bandgap material, the exciton emission, which exists only as a transient excited state, has a much shorter lifetime[13]. Given the 20 times lower measured photoluminescence quantum yield, the observed $\rho = 0.25 \pm 0.05$ indicates that the hole spin lifetime in bilayer MoS_2 is only a few hundreds of femtoseconds.

How do we understand the striking difference of more than three orders of magnitude in the valence hole spin lifetimes in mono- and bilayer MoS_2? The effect is a direct consequence of the different crystal symmetries of the two materials. In monolayers where inversion symmetry is broken, valley and spin are coupled[11,19,20]. σ_- excitation creates excitons with electron spin down ($e_\downarrow$) and hole spin up ($h_\uparrow$) at the K point (Fig. 3c). Intravalley scattering to the $h_\downarrow$ state is forbidden, because the spin degeneracy near the valence-band edge is split by 160 meV. Intervalley scattering from the K to K′ point, which also involves simultaneous spin flip, requires coupling with both atomic-scale scatters (because of the large change of momentum involved) and with magnetic defects (because S_z is a good quantum number). As a result of such restrictions, we expect very long valley-spin lifetimes for holes in monolayer MoS_2 (ref. 11). A more detailed discussion of spin relaxation mechanisms[23,25,26], including the Elliot–Yafet and D'yakonov–Perel' mechanisms, as well as e–h exchange interactions in monolayer MoS_2, is presented in Supplementary Section S3.

In bilayer MoS_2 with Bernal stacking (Fig. 1d), on the other hand, inversion symmetry ($E_\uparrow(\mathbf{k}) = E_\uparrow(-\mathbf{k})$) is restored, and spin and valley are no longer coupled. In combination with time-reversal symmetry ($E_\downarrow(\mathbf{k}) = E_\uparrow(-\mathbf{k})$), spin degeneracy of the bands ($E_\downarrow(\mathbf{k}) = E_\uparrow(\mathbf{k})$) is restored at each valley. The fourfold degenerate valence bands at each valley are split, by the combined spin–orbit interactions in each monolayer and the interlayer interactions, into two spin-degenerate valence bands (Fig. 1e,f). σ_- excitation on resonance with the A exciton generates excitons with $e_\downarrow$ and $h_\uparrow$ in both the K and K′ valleys. There is net spin orientation, but no valley polarization (Fig. 3f). Intravalley hole spin relaxation (from interlayer tunnelling of charge carriers) through the Elliot–Yafet mechanism becomes effective. In addition, relaxation through the D'yakonov–Perel' mechanism can also be effective in substrate-supported bilayer samples with slightly broken inversion symmetry, giving rise to Rashba fields[23,25,26]. A short hole spin lifetime and a small degree of photoluminescence helicity are thus observed.

We now return to monolayer MoS_2 to examine the dynamics of valley-spin polarization from more highly excited states. Figure 3g,h presents the helicity resolved photoluminesence spectra and the corresponding ρ for σ_- excitation well above both the A and B exciton features at 2.33 eV (532 nm). The observed emission is completely unpolarized, implying no valley-spin polarization. This behaviour is understood to be a consequence of the relaxation of the optical selection rules: off-resonance excitation simultaneously populates both K and K′ valleys (Fig. 3i). Figure 3j,k shows corresponding results for excitation of the B exciton at 2.09 eV (594 nm). In this case, according to the optical selection rules[11,12] only K-point excitons are created. Hot luminescence near the B exciton energy does indeed exhibit the same helicity as the optical excitation. However, emission by the A exciton is unpolarized, reflecting the equal population of band-edge holes at the two valleys after relaxation from the B to the A exciton state (Fig. 3l). The variation of photoluminescence helicity with pump photon

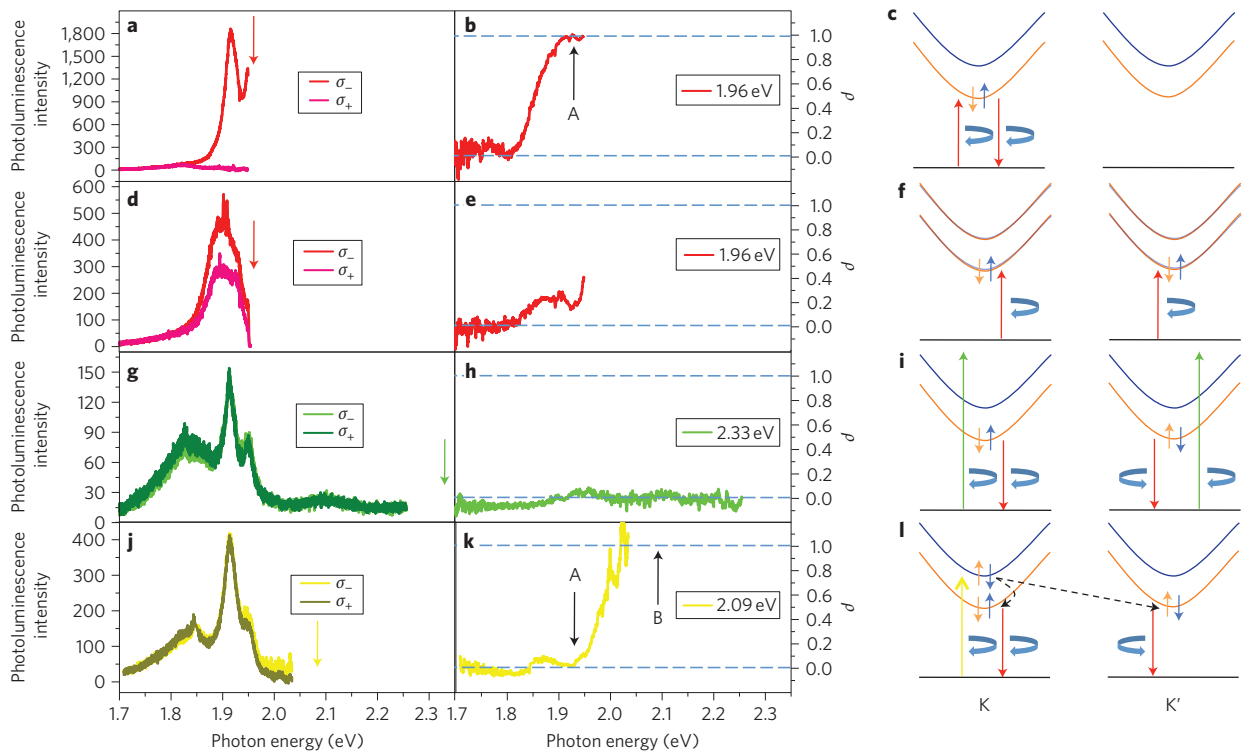

Figure 3 | Optical control of valley-spin polarization in monolayer MoS_2. All optical excitation is left circularly polarized (σ_-). The excitation photon energies are identified by arrows in the left column. **a–c**, Excitation of monolayer MoS_2 at 1.96 eV (633 nm), on resonance with the A exciton. **d–f**, Excitation of bilayer MoS_2 at 1.96 eV. **g–i**, Excitation of monolayer at 2.33 eV (532 nm), off resonance with both the A and B exciton. **j–l**, Excitation of monolayer at 2.09 eV (594 nm), on resonance with the B exciton. Left column: σ_- and σ_+-resolved photoluminescence spectra. Middle column: corresponding photoluminescence helicity as a function of photon energy. Right column: schematic representation of optical absorption and emission processes.

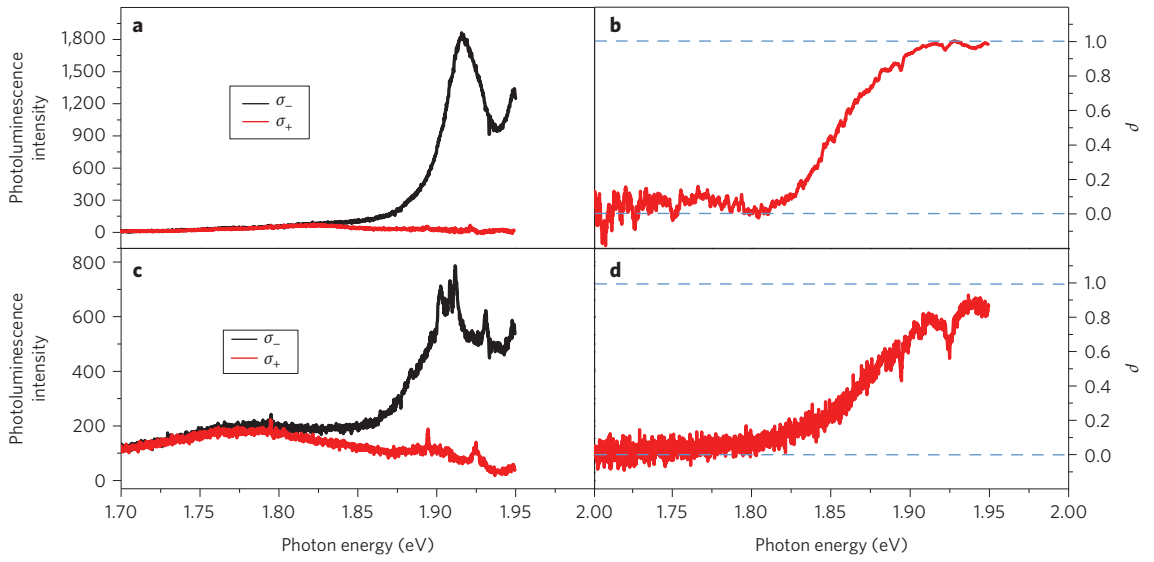

Figure 4 | Substrate-independent photoluminescence helicity. a,**c**, σ_- and σ_+-resolved photoluminescence spectra for monolayer MoS_2 on h-BN (**a**) and on SiO_2/silicon substrates (**c**). **b**,**d**, Corresponding photoluminescence helicity ρ.

energy further supports the interpretation of perfect valley selective excitation in monolayer MoS_2.

The demonstration of full control of valley polarization in monolayer MoS_2 through the helicity of optical pump photons is based on the existence of high-symmetry valleys in a non-centrosymmetric material. The stability of this effect is enhanced by the relatively large spin–orbital interactions associated with the metal *d* orbitals and the perfect two-dimensional confinement that suppresses valley-spin relaxation. We have accordingly also observed similar results in studies of monolayer MoS_2 samples on different substrates (Fig. 4) and over a wide range of temperature (Supplementary Section S4). The robustness of the reported phenomenon opens up a new avenue for the control of valley-spin polarization in solids, with implications both for fundamental studies of valley-spin polarization and for electronic and optoelectronic applications based on these degrees of freedom.

Methods

Sample preparation. Monolayer and bilayer MoS_2 samples of a few micrometres in size were obtained by mechanical exfoliation from a bulk crystal (SPI). We used h-BN substrates for monolayer samples, because this material provided comparatively high photoluminescence quantum yield (or, equivalently, long exciton lifetime). To prepare MoS_2 monolayers on h-BN, thin layers of h-BN were first exfoliated onto SiO_2/silicon substrates, and monolayers of MoS_2 were then transferred onto them[27]. For comparison with samples on SiO_2/silicon, we chose a MoS_2 sample lying on both the BN-covered and bare portion of the SiO_2/silicon substrate. The MoS_2 bilayer samples were deposited on standard SiO_2/silicon substrates.

Optical measurements. The samples were examined using a microscope coupled to a cryostat cooled by liquid helium. For the reflectance contrast measurements, we focused light from a broadband radiation source (Fianium supercontinuum source) onto the samples (spot diameter, ~2 μm) using a ×40 long-working-distance objective. The reflected light was collected by the same objective and guided to a grating spectrometer equipped with a charge-coupled device detector.

The photoluminescence measurements were performed using excitation at three photon energies (arrows in Fig. 2a), corresponding to 1.96 (HeNe laser), 2.09 and 2.33 eV (solid-state lasers) radiation. The sample temperature of 14 K was chosen so that the HeNe line matched the energy of the A exciton. The photoluminescence emission was recorded using the same spectrometer as for the reflectance contrast measurements, but with the scattered laser radiation blocked by suitable long-pass filters. To achieve circularly polarized excitation, the laser radiation was sent through a Babinet–Soleil compensator and the state of circular polarization on the sample location was confirmed. An objective of relatively small numerical aperture (<0.5) was used to achieve close-to-normal-incidence excitation with negligible photon angular momentum in the sample in-plane direction.

The desired helicity of the collected photoluminescence was selected by sending the emission through a quarter-wave Fresnel rhomb (a broadband circular polarizer) followed by a linear polarizer. The circular polarization state of the photoluminescence was slightly distorted after passing through the microscope. We therefore corrected the measured photoluminescence helicity parameter ρ by normalizing it with respect to the handedness ρ_0 of the scattered laser light detected in the same fashion. This radiation was known to be circularly polarized, so the slight departure of ρ_0 from unity could be attributed to birefringence in the collection optics. In this calibration procedure, we ignored dispersion effects. This is justified given the small Stokes shift of the photoluminescence features from the excitation laser wavelength. As a further check, we excited the sample with linearly polarized light (both *s*- and *p*-polarized) and detected left and right circularly polarized photoluminescence spectra. As expected, they were fully equivalent under these conditions.

Received 10 April 2012; accepted 10 May 2012;
published online 17 June 2012

References

1. Rycerz, A., Tworzydlo, J. & Beenakker, C. W. J. Valley filter and valley valve in graphene. *Nature Phys.* **3,** 172–175 (2007).
2. Akhmerov, A. R. & Beenakker, C. W. J. Detection of valley polarization in graphene by a superconducting contact. *Phys. Rev. Lett.* **98,** 157003 (2007).
3. Xiao, D., Yao, W. & Niu, Q. Valley-contrasting physics in graphene: magnetic moment and topological transport. *Phys. Rev. Lett.* **99,** 236809 (2007).
4. Yao, W., Xiao, D. & Niu, Q. Valley-dependent optoelectronics from inversion symmetry breaking. *Phys. Rev. B* **77,** 235406 (2008).
5. Gunawan, O. *et al.* Valley susceptibility of an interacting two-dimensional electron system. *Phys. Rev. Lett.* **97,** 186404 (2006).
6. Takashina, K., Ono, Y., Fujiwara, A., Takahashi, Y. & Hirayama, Y. Valley polarization in Si(100) at zero magnetic field. *Phys. Rev. Lett.* **96,** 236801 (2006).
7. Shkolnikov, Y. P., De Poortere, E. P., Tutuc, E. & Shayegan, M. Valley splitting of AlAs two-dimensional electrons in a perpendicular magnetic field. *Phys. Rev. Lett.* **89,** 226805 (2002).
8. Bishop, N. C. *et al.* Valley polarization and susceptibility of composite fermions around a filling factor ν=3/2. *Phys. Rev. Lett.* **98,** 266404 (2007).
9. Eng, K., McFarland, R. N. & Kane, B. E. Integer quantum Hall effect on a six-valley hydrogen-passivated silicon (111) surface. *Phys. Rev. Lett.* **99,** 016801 (2007).
10. Zhu, Z., Collaudin, A., Fauque, B., Kang, W. & Behnia, K. Field-induced polarization of Dirac valleys in bismuth. *Nature Phys.* **8,** 89–94 (2012).
11. Xiao, D., Liu, G. B., Feng, W., Xu, X. & Yao, W. Coupled spin and valley physics in monolayers of MoS_2 and other group-VI dichalcogenides. *Phys. Rev. Lett.* **108,** 196802 (2012).
12. Cao, T., Feng, J., Shi, J., Niu, Q. & Wang, E. MoS_2 as an ideal material for valleytronics: valley-selective circular dichroism and valley Hall effect. Preprint at http://arxiv.org/abs/1112.4013 (2011).
13. Mak, K. F., Lee, C., Hone, J., Shan, J. & Heinz, T. F. Atomically thin MoS_2: a new direct-gap semiconductor. *Phys. Rev. Lett.* **105,** 136805 (2010).
14. Splendiani, A. *et al.* Emerging photoluminescence in monolayer MoS_2. *Nano Lett.* **10,** 1271–1275 (2010).

15. Lebegue, S. & Eriksson, O. Electronic structure of two-dimensional crystals from *ab initio* theory. *Phys. Rev. B* **79,** 115409 (2009).
16. Li, T. & Galli, G. Electronic properties of MoS_2 nanoparticles. *J. Phys. Chem. C* **111,** 16192–16196 (2007).
17. Zeng, H., Dai, J., Wang, Y., Xiao, D. & Cui, X. Valley polarization in MoS_2 monolayers by optical pumping. *Nature Nanotech.* http://dx.doi.org/10.1038/nnano.2012.95 (2012).
18. Mattheiss, L. F. Band structures of transition-metal–dichalcogenide layer compounds. *Phys. Rev. B* **8,** 3719–3740 (1973).
19. Zhu, Z. Y., Cheng, Y. C. & Schwingenschlogl, U. Giant spin-orbit-induced spin splitting in two-dimensional transition-metal dichalcogenide semiconductors. *Phys. Rev. B* **84,** 153402 (2011).
20. Cheiwchanchamnangij, T. & Lambrecht, W. R. L. Quasiparticle band structure calculation of monolayer, bilayer, and bulk MoS_2. *Phys. Rev. B* **85,** 205302 (2012).
21. Kheng, K. *et al.* Observation of negatively charged excitons X^- in semiconductor quantum wells. *Phys. Rev. Lett.* **71,** 1752–1755 (1993).
22. Radisavljevic, B., Radenovic, A., Brivio, J., Giacometti, V. & Kis, A. Single-layer MoS_2 transistors. *Nature Nanotech.* **6,** 147–150 (2011).
23. Dyakonov, M. I. *Spin Physics in Semiconductors* (Springer, 2008).
24. Korn, T., Heydrich, S., Hirmer, M., Schmutzler, J. & Schueller, C. Low-temperature photocarrier dynamics in monolayer MoS_2. *Appl. Phys. Lett.* **99,** 102109 (2011).
25. Zutic, I., Fabian, J. & Das Sarma, S. Spintronics: fundamentals and applications. *Rev. Mod. Phys.* **76,** 323–410 (2004).
26. Meier, F. & Zakharchenya, B. P. *Optical Orientation* (North-Holland, 1984).
27. Dean, C. R. *et al.* Boron nitride substrates for high-quality graphene electronics. *Nature Nanotech.* **5,** 722–726 (2010).

Acknowledgements

This research was supported by the National Science Foundation (grant DMR-1106172 at Columbia University and grant DMR-0907477 at Case Western Reserve University). Additional support for the optical instrumentation at Columbia University was provided by the Center for Re-Defining Photovoltaic Efficiency Through Molecule Scale Control, an Energy Frontier Research Center funded by the US Department of Energy (DOE), Office of Basic Energy Sciences (grant DE-SC0001085). The authors thank G.H. Lee and J. Hone for help with sample preparation and I. Aleiner, W. Lambrecht and P. Kim for fruitful discussions.

Author contributions

K.F.M. and J.S. developed the concept, designed the experiment and prepared the manuscript. K.F.M. performed the polarization resolved photoluminescence measurements. K.H. prepared the samples and contributed to the study of temperature dependence. All authors contributed to the interpretation of the results and writing the manuscript.

Additional information

The authors declare no competing financial interests. Supplementary information accompanies this paper at www.nature.com/naturenanotechnology. Reprints and permission information is available online at http://www.nature.com/reprints. Correspondence and requests for materials should be addressed to T.F.H.